Large spectral extinction due to overlap of dipolar and quadrupolar plasmonic modes of metallic nanoparticles in arrays

Christopher P. Burrows* and William L. Barnes

School of Physics, University of Exeter, Stocker Road, Exeter, EX4 4QL, United Kingdom.
**c.p.burrows@ex.ac.uk*

Abstract: We explore the optical response of two-dimensional (2D) arrays of silver nanoparticles, focussing our attention on structures for which the individual particles in isolation support both dipolar and quadrupolar localised surface plasmon modes. For individual spheres we show that when dipolar and quadrupolar modes are excited simultaneously, interference leads to most of the scattered light being radiated in the forward direction. This is in contrast to what happens when each mode is excited on its own. We further show, using finite-element modelling that when such particles are assembled into square 2D arrays, the dipolar and quadrupolar modes can combine to produce a single peak in the optical density of the array. By simulating the field distributions associated with these modes we are able to illustrate the dual-mode character of this feature in the optical density. We have extended our examination of this effect by considering how the optical density of these arrays changes with incident angle for two polarisations (*s* and *p*).

OCIS codes: (250.5403) Plasmonics; (160.3918) Metamaterials; (350.4238) Nanophotonics and photonic crystals

References and links

1. E. Hutter, and J. H. Fendler, "Exploitation of localized surface plasmon resonance," Adv. Mater. **16**(19), 1685–1706 (2004).
2. W. A. Murray, and W. L. Barnes, "Plasmonic materials," Adv. Mater. **19**(22), 3771–3782 (2007).
3. G. A. Wurtz, P. R. Evans, W. Hendren, R. Atkinson, W. Dickson, R. J. Pollard, A. V. Zayats, W. Harrison, and C. Bower, "Molecular plasmonics with tunable exciton-plasmon coupling strength in J-aggregate hybridized Au nanorod assemblies," Nano Lett. **7**(5), 1297–1303 (2007).
4. F. J. G. de Abajo, "Colloquium: Light scattering by particle and hole arrays," Rev. Mod. Phys. **79**(4), 1267–1290 (2007).
5. G. Vecchi, V. Giannini, and J. Gómez Rivas, "Shaping the Fluorescent Emission by Lattice Resonances in Plasmonic Crystals of Nanoantennas," Phys. Rev. Lett. **102**(14), 146807 (2009).
6. S. L. Zou, and G. C. Schatz, "Narrow plasmonic/photonic extinction and scattering line shapes for one and two dimensional silver nanoparticle arrays," J. Chem. Phys. **121**(24), 12606–12612 (2004).
7. A. N. Grigorenko, A. K. Geim, H. F. Gleeson, Y. Zhang, A. A. Firsov, I. Y. Khrushchev, and J. Petrovic, "Nanofabricated media with negative permeability at visible frequencies," Nature **438**(7066), 335–338 (2005).
8. Y. Z. Chu, E. Schonbrun, T. Yang, and K. B. Crozier, "Experimental observation of narrow surface plasmon resonances in gold nanoparticle arrays," Appl. Phys. Lett. **93**(18), 181108 (2008).
9. N. I. Zheludev, S. L. Prosvirnin, N. Papasimakis, and V. A. Fedotov, "Lasing spaser," Nat. Photonics **2**(6), 351–354 (2008).
10. G. Mie, "Beiträge zur Optik trüber Medien, speziell kolloidaler Metallösungen," Ann. Phys. **330**(3), 377–445 (1908).
11. J. A. Stratton, *Electromagnetic Theory* (McGraw-Hill, New York, 1941).
12. C. F. Bohren, and D. R. Huffman, *Absorption and Scattering of Light by Small Particles* (Wiley, New York, 1983).
13. U. Kreibig, and M. Vollmer, *Optical Properties of Metal Clusters* (Springer-Verlag, Berlin, 1995).
14. K. Lindfors, T. Kalkbrenner, P. Stoller, and V. Sandoghdar, "Detection and spectroscopy of gold nanoparticles using supercontinuum white light confocal microscopy," Phys. Rev. Lett. **93**(3), 037401 (2004).

#120946 - $15.00 USD Received 4 Dec 2009; revised 12 Jan 2010; accepted 12 Jan 2010; published 29 Jan 2010

15. E. D. Palik, *Handbook of Optical Constants and Solids* (Academic Press Inc., London, 1985).
16. W. J. Wiscombe, "Improved Mie Scattering Algorithms," Appl. Opt. **19**(9), 1505–1509 (1980).
17. S. J. Oldenburg, G. D. Hale, J. B. Jackson, and N. J. Halas, "Light scattering from dipole and quadrupole nanoshell antennas," Appl. Phys. Lett. **75**(8), 1063–1065 (1999).
18. C. L. Haynes, A. D. McFarland, L. L. Zhao, R. P. Van Duyne, G. C. Schatz, L. Gunnarsson, J. Prikulis, B. Kasemo, and M. Kall, "Nanoparticle optics: The importance of radiative dipole coupling in two-dimensional nanoparticle arrays," J. Phys. Chem. B **107**(30), 7337–7342 (2003).
19. W. Rechberger, A. Hohenau, A. Leitner, J. R. Krenn, B. Lamprecht, and F. R. Aussenegg, "Optical properties of two interacting gold nanoparticles," Opt. Commun. **220**(1-3), 137–141 (2003).
20. S. Malynych, and G. Chumanov, "Light-induced coherent interactions between silver nanoparticles in two-dimensional arrays," J. Am. Chem. Soc. **125**(10), 2896–2898 (2003).
21. F. Hao, Y. Sonnefraud, P. Van Dorpe, S. A. Maier, N. J. Halas, and P. Nordlander, "Symmetry Breaking in Plasmonic Nanocavities: Subradiant LSPR Sensing and a Tunable Fano Resonance," Nano Lett. **8**(11), 3983–3988 (2008).
22. B. N. Khlebtsov, V. A. Khanadeyev, J. Ye, D. W. Mackowski, G. Borghs, and N. G. Khlebtsov, "Coupled plasmon resonances in monolayers of metal nanoparticles and nanoshells," Phys. Rev. B **77**(3), 035440 (2008).
23. J. Jackson, *Classical Electrodynamics* (Wiley, New York, 1962).
24. D. V. Vezenov, B. T. Mayers, D. B. Wolfe, and G. M. Whitesides, "Integrated fluorescent light source for optofluidic applications," Appl. Phys. Lett. **86**(4), 041104 (2005).
25. S. Zhang, D. A. Genov, Y. Wang, M. Liu, and X. Zhang, "Plasmon-induced transparency in metamaterials," Phys. Rev. Lett. **101**(4), 047401 (2008).
26. D. M. Pozar, *Microwave Engineering* (John Wiley & Sons, Hoboken, 2005).

1. Introduction

The scattering of light by metallic nanoparticles has seen a recent resurgence of interest in the field of plasmonics [1, 2]. Sub-wavelength arrays of metal nanostructures are particularly fascinating owing to the greater range of phenomena they exhibit [3–8]. They form the basis of some of the structures pursued in the development of electromagnetic metamaterials [9]. In this study we are interested in dipolar and higher order (multipolar) modes of metallic nanospheres and the manner in which these modes interact when the nanospheres are brought together. The optical properties of arrays of metal nanoparticles have been studied before, however, most studies are concerned only with dipolar modes, higher order modes are less studied, and often ignored. In this work we are particularly interested in the response of square arrays of silver nanospheres in which the nanospheres are large enough to support both dipolar and quadrupolar modes. We first look at the localised surface plasmon modes of individual metal nanospheres. We then extend our discussion to examine the optical response of square, 2D arrays of silver nanospheres.

2. Localised surface plasmon modes of individual metal nanospheres

The scattering and absorption of light by a spherical object with known material parameters is described exactly by Mie theory [10–12]. In this theory, the vector spherical harmonics of the scattered field are expressed in the form of a multipole expansion, the first term representing the dipolar mode, the second representing the quadrupolar mode, and so on. For very small silver spheres (d<50 nm), only the dipolar mode can be excited by light at optical frequencies due to the metallic response having an upper bound in frequency [13]. This mode can lead to strong scattering of light by the particle in directions normal to the induced oscillating dipole moment. Strong absorption may also begin to dominate the response as the diameter becomes smaller than 50 nm [14]. As the size of the particle is increased, the particle may also support a quadrupolar mode. To couple incident light to the quadrupolar mode requires the phase of the incident light to change significantly across the particle. Thus incident light is most easily coupled to quadrupoles that lie in the plane defined by the **E**-field and **k**-vector of the incident light. Higher frequencies enable rapid spatial changes in phase so that, for a given nanosphere, quadrupolar modes are expected to occur at higher frequencies than dipolar modes.

The dipolar and quadrupolar modes appear as peaks in the extinction and scattering spectra of a 100 nm diameter silver sphere surrounded by glass (n=1.5). This is shown in Fig.

#120946 - $15.00 USD Received 4 Dec 2009; revised 12 Jan 2010; accepted 12 Jan 2010; published 29 Jan 2010

1 where extinction and scattering spectra are presented, these data were calculated using Mie theory, the permittivity of silver being taken from the literature [15]. The dipolar mode appears at a wavelength of 548 nm and the quadrupolar mode appears at 427 nm.

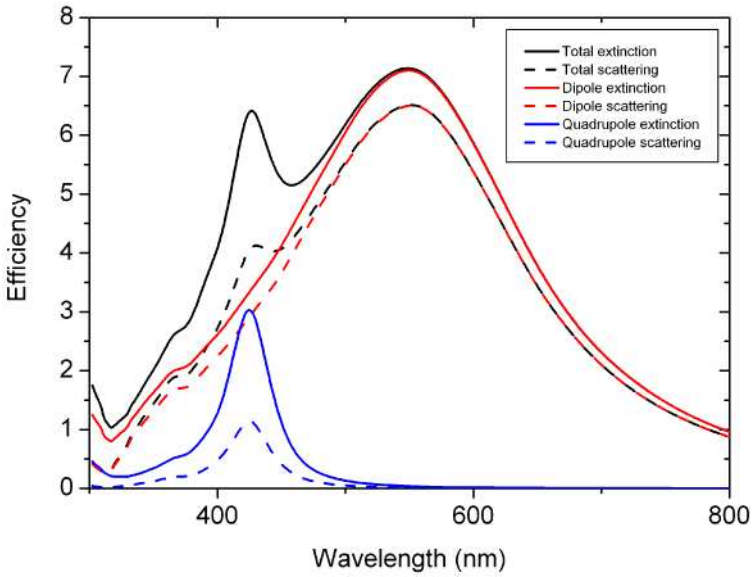

Fig. 1. Spectra calculated using Mie theory showing the extinction and scattering efficiencies of a 100 nm diameter silver sphere surrounded by glass (n=1.5). Permittivity values for silver were taken from the literature [15] and interpolated with a spline fit. The spectral features of the dipolar and quadrupolar modes are at 548 nm and 427 nm respectively. Also shown are the sets of spectra obtained when the calculation is carried out but only considering single modes – the dipole in red or the quadrupole in blue. Additional features in the spectra below 400 nm arise from fluctuations in the permittivity values and are not plasmonic effects.

The results obtained from Mie theory are produced by first expanding the incident plane-wave in terms of vector spherical harmonics, and then calculating the value of the overlap integral between this expression and the vector spherical harmonics which describe the separate modes supported by the particle (calculated by solving Laplace's equation in spherical polar coordinates and applying orthogonality conditions). The values of these integrals lead to the weighting coefficients which describe how well incident light of a particular wavevector can couple to the modes. Imposing appropriate boundary conditions on the internal and external fields, we can determine explicit expressions for the internal and scattered fields [12]. The expressions for the angular dependence of the scattered fields are:

$$E_\theta \approx E_0 \frac{e^{ikr}}{-ikr}\cos\varphi \sum_n \frac{2n+1}{n(n+1)}\left(a_n \frac{dP_n^1}{d\theta} + b_n \frac{P_n^1}{\sin\theta}\right) \quad (1)$$

$$E_\varphi \approx -E_0 \frac{e^{ikr}}{-ikr}\sin\varphi \sum_n \frac{2n+1}{n(n+1)}\left(a_n \frac{P_n^1}{\sin\theta} + b_n \frac{dP_n^1}{d\theta}\right) \quad (2)$$

Here, E_θ and E_φ are the complex scattered electric fields in the far-field, E_0 is the strength of the incident field, k is the wavevector, θ and φ are the polar and azimuthal scattering angles respectively, n defines the degree of the mode (i.e. for the dipolar mode n=1, for the quadrupolar mode n=2 etc.). The symbol P_n^1 represents the set of associated Legendre polynomials of order 1, and a_n and b_n are the complex Mie coefficients calculated by

#120946 - $15.00 USD Received 4 Dec 2009; revised 12 Jan 2010; accepted 12 Jan 2010; published 29 Jan 2010

evaluating the overlap integral between the incident field and the field associated with the natural modes of the system.

In order to achieve a good balance between accuracy and speed in carrying out these calculations, the series expansions in Eq. (1) and Eq. (2) are truncated after a certain number of terms. The order, n, at which the truncation takes place is determined from the size parameter, x, by taking the nearest integer to $x + 4x^{1/3} + 2$ (the size parameter, x, is given by $x=ka$, where k is the wavevector in the surrounding medium and a is the particle radius) [16]. The results from the Mie calculations can be used to calculate the scattering, absorption and extinction efficiencies at each wavelength. Once the expansion has been made, it is possible to isolate individual modes in order to examine their characteristics, and this is achieved by simply setting the weighting coefficients (the a_n and b_n in Eq. (1) and Eq. (2)) of all other modes to be equal to zero. The individual components (dipolar and quadrupolar) of the extinction and scattering spectra for a 100 nm diameter silver sphere surrounded by glass have been calculated in this way and are shown in Fig. 1, along with the total contribution from all modes. At the frequency of the quadrupolar mode we see that the extinction is due to a mixture, roughly equal, of dipolar and quadrupolar contributions.

Further insight into the scattering of light by a metal nanosphere can be gained from an examination of the field distributions associated with the supported modes. As stated previously, Mie theory allows us to isolate expressions for the scattered field in terms of vector spherical harmonics for the different modes. This allows us to calculate and plot the angular distribution of the scattered light based on Eq. (1) and Eq. (2). The data in Fig. 2 show the angular dependence of the relative intensity of light scattered into the far-field by a 100 nm diameter silver sphere in glass for the dipolar and quadrupolar modes in isolation, and for the quadrupolar mode with several terms considered in the series expansion. It can be seen that the dipolar mode leads to strong scattering in directions that are orthogonal to the polarisation of the incident light [11]. The quadrupolar mode scatters strongly into four lobes – two along the axis of the incident wavevector, and the other two along the axis of the incident electric field.

#120946 - $15.00 USD Received 4 Dec 2009; revised 12 Jan 2010; accepted 12 Jan 2010; published 29 Jan 2010

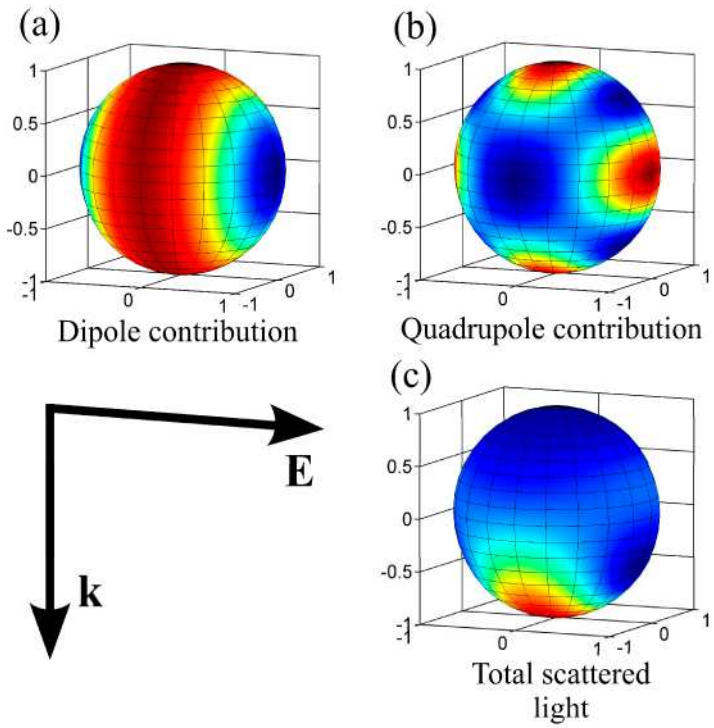

Fig. 2. Far-field scattered intensity profiles calculated from Mie theory for a 100 nm diameter silver sphere surrounded by glass. The relative scattering intensity is shown for (a) a pure dipolar mode, (b) a pure quadrupolar mode and (c) the quadrupole frequency with contributions from all modes included. The colour-scale of each plot is normalised so that the maximum scattered intensity is unity for each.

Interestingly, when one considers scattering at the frequency of the quadrupolar mode of this particle, taking several terms of the expansion (Eq. (1) and Eq. (2)) into account, the scattered light is found to be almost entirely in the forward direction. At first this may seem somewhat surprising since the dipolar mode radiates equally in both the forward and backward directions, as does the quadrupolar mode. As noted above, the scattering spectrum shows that there is still a significant contribution to scattering at the quadrupole frequency from the dipolar mode of a particle when the dipolar and higher order terms are taken into consideration. Also, the lobes of the quadrupolar mode in the direction of the incident electric field do not appear in the plot when several modes are included in the calculation as their intensities are small compared to the forward-scattered light and so are not seen in the colour-plot. In studies of far-field angular scattering it is often the case that only the intensity is taken into consideration as it is the experimentally measurable quantity [17]. The scattering intensities considered in the present study have components from several eigenmodes, and the fields of these modes all contribute to the two components of the electric field (E_θ and E_φ) in the far-field. These fields are complex, and it is only by considering the amplitude and phase of the fields at each point that it is possible to begin to understand the interference between the radiation of multiple modes at a particular frequency which gives rise to a particular scattering intensity distribution. This is important as it is the sum of the complex fields which is used to calculate the total intensity, not the sum of the intensities of the individual modes. It should be noted that in a spherical polar coordinate system, the angular unit vectors are angle dependent and care is needed when discussing the sign of the fields in the forward- and back-scattered directions (see Appendix 1). When the complex fields of all modes are added together for the quadrupolar frequency, the dipolar and quadrupolar modes

#120946 - $15.00 USD Received 4 Dec 2009; revised 12 Jan 2010; accepted 12 Jan 2010; published 29 Jan 2010

interfere constructively in the forward direction and destructively in the backward direction, leading to the intensity distribution shown in Fig. 2(c).

3. Interparticle coupling in 2D arrays of metal spheres

When two particles are separated by distances much greater than the wavelength of incident light, the system can be treated as a multiple scattering problem, there is no near-field interaction between the particles. For separations comparable with the wavelength of light, coherent, radiative coupling of the particles is possible. For still closer separations near-field coupling can occur. The effects of near-field and radiative coupling were investigated by Haynes *et al.* [18] for the specific case of regular arrays of metal discs illuminated at normal incidence. A blue shift in the resonance frequency of the in-plane dipolar mode was observed as the interparticle separation was reduced. However for separations less than some critical value the resonance shifted back to the red. The initial blue-shift in the collective response occurs because the dipolar modes of each particle radiate in the y-direction (see Fig. 3), and these fields perturb the modes of their neighbours, leading to an increase in the restoring force on the electrons, thus increasing the frequency of the mode of the collective system. In contrast, when the particles are very close, the near-fields, which have short decay lengths, begin to dominate the perturbation by means of interactions along the axis of the incident electric field (the x-direction). The restoring force is thus weakened, leading to a red-shift in frequency of the dipolar mode [19].

Here we are primarily interested in arrays of spherical particles (Fig. 3) which exhibit spectral features due to quadrupolar modes in addition to the dipolar modes. The particle arrays studied by Haynes *et al*. only exhibited dipolar modes, even though the particles were large enough to support quadrupolar modes in the plane of the disc. The arrays were, however, illuminated at normal incidence so there was no phase retardation in a plane which would allow the incident light to couple to this in-plane quadrupolar mode. Malynych and Chumanov [20] presented results of extinction measurements from a random array of silver spheres dispersed in a polymer film. They varied the interparticle separation and at short separations observed a strong peak in the optical density at a wavelength corresponding to the quadrupolar mode of the single-particle extinction spectrum. Malynych and Chumanov attributed this large extinction to in-plane, coherent coupling of quadrupolar modes associated with the silver nanospheres. As discussed above, however, the excitation of a quadrupolar mode relies on phase retardation from one side of the particle to the other. For normal incidence it is thus not possible to couple to an in-plane quadrupolar mode, and yet it is an normal incidence that Malynych and Chumanov observed their strongest extinction [20]. Furthermore, if this in-plane coherent interaction was the cause of the single strong peak observed by Malynych and Chumanov, one would have expected Haynes *et al*. to have observed similar effects in the optical response of their arrays of discs. It is possible that in the case of a disordered array, isolated instances of broken symmetry could give rise to the in-plane excitation of a quadrupolar mode [21] due to particles scattering normally incident light into the plane of the array. Whilst this symmetry breaking may change the optical density spectrum slightly, similar spectral features were observed in exact simulations of ordered finite arrays of particles, demonstrating that the effect is not solely dependent on the presence of disorder [22].

#120946 - $15.00 USD Received 4 Dec 2009; revised 12 Jan 2010; accepted 12 Jan 2010; published 29 Jan 2010

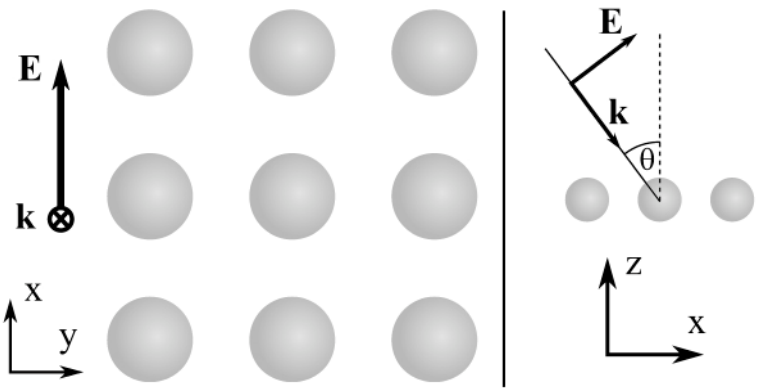

Fig. 3. A schematic showing a small portion of an infinite square array of metal nanoparticles such as those considered in this study. The directions associated with normally incident light are indicated (left), as well as the directions for p-polarised light at oblique incidence to the array (right).

In order to understand better the physical mechanisms for the spectral response of these arrays, we present results from finite-element modelling (see Appendix 2) which allow spectral features to be discussed with reference to their associated electric field distributions. Figure 4 shows the calculated optical density of a square array of 100 nm diameter silver spheres on a square lattice surrounded by glass for a range of array periods. It can be seen that when the separation is as large as possible whilst still ensuring the diffraction edge (separation=255 nm) lies outside the spectral range of interest, the spectrum has two distinct peaks. The peak at the longer wavelength, 500 nm, corresponds to the dipolar mode whilst the peak at 428 nm corresponds to the quadrupolar mode. The dipolar peak is shifted compared to the single particle spectrum (Fig. 1) due to radiative coupling between the particles, as observed by Haynes *et al.* [18] for discs. The wavelength of the quadrupolar mode, however, remains practically unchanged. This is because the decay length of the quadrupolar field is very short compared to that of the dipolar mode [23], so the frequency of the quadrupolar mode is not significantly perturbed by the presence of neighbours.

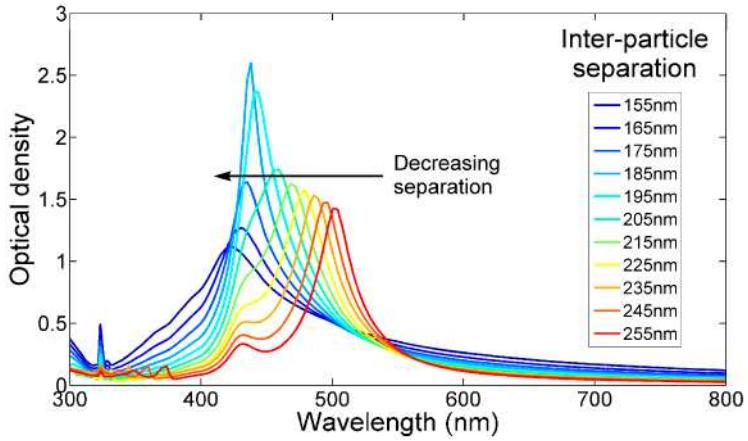

Fig. 4. Optical density spectra of infinite square arrays of silver nanospheres (100 nm diameter) surrounded by glass for a range of array periods as calculated using a finite-element method (see Appendix 2). The arrays with the largest periods show two clear features, those of the dipolar and the quadrupolar modes. Closer separations show just one peak corresponding to the dual-mode resonance. The features below 375 nm are mainly due to diffraction effects.

#120946 - $15.00 USD Received 4 Dec 2009; revised 12 Jan 2010; accepted 12 Jan 2010; published 29 Jan 2010

Finite-element modelling has allowed us to unambiguously attribute the spectral peaks to be the dipolar and quadrupolar modes by examination of the electric field distributions inside the spheres. Time averaged field magnitudes provide sufficient information to be able to identify the modes, but animations of the field vectors give a better illustration of the nature of the modes (Fig. 5).

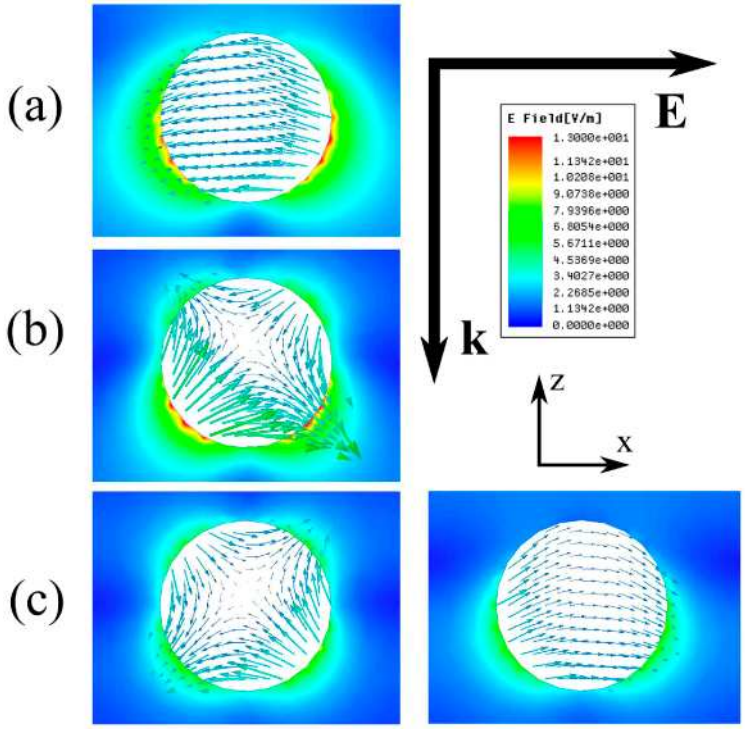

Fig. 5. Simulated electric field profiles for infinite square arrays of 100 nm diameter silver spheres in glass. Shown in each plot is the magnitude of the real part of the total electric field in the glass surrounding the sphere at a single phase in the x-z plane, and arrows showing the direction and strength of the total electric field inside the sphere. These plots are for (a) a 255 nm period array calculated at a wavelength of 500 nm, corresponding to the dipolar mode (Media 1), (b) 255 nm period at a wavelength of 428 nm, corresponding to the quadrupolar mode (Media 2), and (c) a 185 nm period at a wavelength of 436 nm, corresponding to the single spectral feature of the short-period system (Media 3). (c) shows the instantaneous electric field profile for two different phases separated by 180°.

At large separations the simulated field plots show either purely dipolar (Fig. 5(a), Media 1) or purely quadrupolar (Fig. 5(b), Media 2) character at the wavelengths corresponding to the spectral peaks, and the modes, therefore are reasonably distinct, as we may expect from considering the corresponding spectrum. As discussed previously for individual particles, there will be weak contributions from the other modes but the near-field plots will be dominated by whichever mode is in resonance. As the particle separation is reduced, the spectral feature corresponding to the dipolar mode blue-shifts due to radiative coupling, and eventually overlaps with the quadrupolar mode which does not shift significantly throughout the set of spectra shown in Fig. 4. The extent of this overlap continues to increase until there is only one spectral feature present (185 nm period). The dual-mode character of this feature can be seen in animations of the electric field vectors within the spheres which show both dipolar and quadrupolar character at different phases of the optical cycle (Fig. 5(c), Media 3). For separations less than 185 nm, the optical density falls and shifts further to the blue. Analysis for separations below 155 nm was complicated by what appears to be the

#120946 - $15.00 USD Received 4 Dec 2009; revised 12 Jan 2010; accepted 12 Jan 2010; published 29 Jan 2010

involvement of higher order modes and stronger near-field interactions. It should be noted that these field plots (Fig. 5) are in the plane containing the incident **k**-vector and incident **E**-field. The plane which was previously thought to contain the quadrupolar mode [20], the x-y plane shows a purely dipolar character due to the lack of phase retardation in this plane as discussed above (Fig. 6, Media 4).

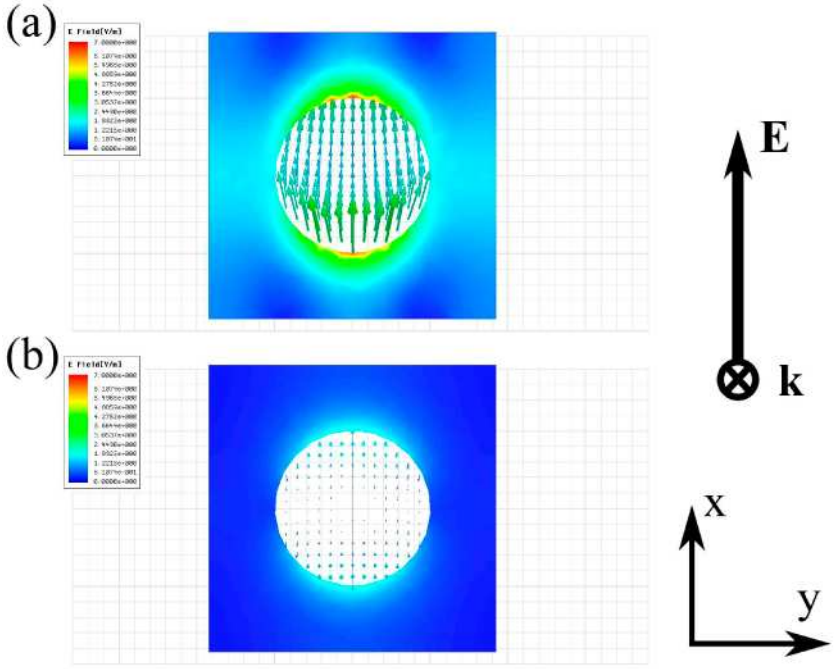

Fig. 6. Simulated electric field profiles for infinite square arrays of 100 nm diameter silver spheres in glass. Shown in each plot is the magnitude of the real part of the total electric field in the glass surrounding the sphere out to the limits of the unit cell, and arrows showing the direction and strength of the total electric field inside the sphere in the x-y plane. These plots are for a 185 nm period at a wavelength of 436 nm, corresponding to the single spectral feature of the short-period system at two different phases of the optical cycle separated by 180° ((a) and (b)). An animation of the complete optical cycle is shown in Media 4.

Further simulations allow us to explore the response of such arrays when illuminated at oblique incidence.

4. Varying the incident angle

When a dense, ordered array of metal nanoparticles is illuminated at an oblique angle, the optical response is very different for p- and s-polarised light due to the very different field configurations. We numerically investigated the angle dependence of the plasmonic interactions by using finite-element modelling to simulate a square array (185 nm array period) of 100 nm silver spheres embedded in a medium of refractive index 1.41 (the same as the PDMS used in [20], the value taken from [24]) as a function of incident angle for both polarisations. At normal incidence, the interaction is coherent and acts to blue-shift the dipolar resonance, as stated above, but away from the normal, the response may be considerably different. In the case of s-polarised illumination, the incident **E**-field is always in the y-direction (see Fig. 3) regardless of incident angle, so there is strong dipolar scattering in the x-z plane. As the angle of incidence is increased, however, there will be de-phasing of the incident field in the x-direction, which is the direction in which the radiative interactions take place, and hence these interactions will be weakened and the blue-shift of the dipolar

#120946 - $15.00 USD Received 4 Dec 2009; revised 12 Jan 2010; accepted 12 Jan 2010; published 29 Jan 2010

mode will be reduced in its magnitude. The spectra in Fig. 7(b) demonstrate this, as for higher angles, the single spectral peak for normal incidence splits into the two separate peaks of the dipolar and quadrupolar modes in a similar way to that seen for the arrays which were illuminated at normal incidence as the array period was increased (Fig. 4).

For p-polarised light the field configuration leads to a markedly different optical response. The incident **E**-field is in the x-z plane for all angles of incidence, and so for all angles, the dipolar mode scatters light in the y-direction, and there is no de-phasing. Along this axis, for all incident angles, there are neighbouring particles which allow strong radiative coupling to take place. Thus for all angles only one spectral peak is seen, the blue-shift of the dipolar mode remains present for all angles of incidence (Fig. 7(a)). Note that the effect of changing the polarisation is very different to the experimental measurements reported by Malynych and Chumanov whose data show the opposite behaviour.

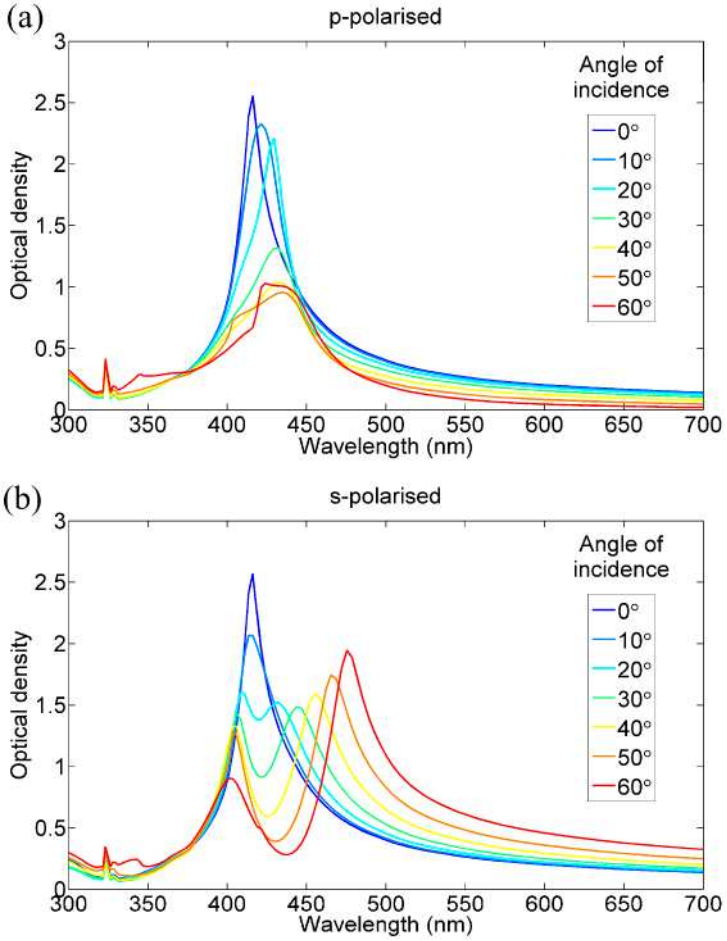

Fig. 7. Optical density of a square array of 100 nm diameter silver nanospheres embedded in PDMS (n=1.41) for a range of incident angles as calculated by finite element modelling for both p- and s-polarised light ((a) and (b) repectively). When the light is p-polarised, there is significant radiative coupling between neighbouring particles which keeps the frequency of the dipolar mode blue-shifted relative to the single-particle case. For s-polarised light, there is significantly less interparticle coupling due to the phase retardation of incident light across the array. This effect is more significant at higher angles, and the two peaks corresponding to the dipole and quadrupolar modes are recovered.

#120946 - $15.00 USD Received 4 Dec 2009; revised 12 Jan 2010; accepted 12 Jan 2010; published 29 Jan 2010

5. Summary

We have shown that for individual particles, the dipolar and quadrupolar modes both contribute to the far-field angular scattering profile at the quadrupole frequency, and the resulting preferential forward scattering occurs as a result of constructive interference of the radiation of the two modes in the forward direction and destructive interference in the backward direction.

Finite-element modelling has provided results which show that the collective behaviour of a square array of 100 nm diameter silver nanospheres surrounded by glass can differ strongly from the behaviour of individual nanospheres. Rather than two distinct modes in the extinction spectrum corresponding to the dipolar and quadrupolar modes (as present in the single particle spectrum), there is just one peak in the optical density of a 185 nm period array with the two modes occurring at very similar frequencies. The mechanism which gives rise to this effect is that the presence of neighbouring plasmonic particles radiatively perturbs the collective dipolar mode of the array, and upon reducing the period of the array, this collective dipolar mode shifts to the blue until it overlaps with the quadrupolar mode. The single spectral peak observed in this study is in good agreement with experimental data in the literature [20], yet the field plots presented here suggest an alternative explanation for the existence of the single peak. We propose that for a particular particle separation the dipolar and quadrupolar modes occur at approximately the same frequency and the contributions of the two modes sum to produce the strong response. It should be noted that the currents primarily associated with the quadrupolar mode occur in a plane normal to the plane of the array rather than in the plane of the array as suggested in the literature [20].

We have extended this study to show that our explanation of the single spectral feature observed at normal incidence can easily be extended to describe the features in the spectra at oblique incidence for both polarisations.

Our results show that higher order modes can significantly modify the optical response of metal nanoparticle arrays. With arrays of metallic nanostructures being considered for a range of metallic electromagnetic metamaterials, an appreciation of the role of higher order modes may be important [9, 25]. We also note that proximity effects between particles in an array can be used to tune the optical response of the array.

Appendix 1

Visualising the complex fields can be quite confusing since the direction of the angular unit vectors in a spherical polar coordinate system are angle-dependent, and, for example, at $(\phi = 0°, \theta = 0°)$, $\hat{\mathbf{e}}_\theta = \hat{\mathbf{e}}_x$ and at $(\phi = 0°, \theta = 180°)$, $\hat{\mathbf{e}}_\theta = -\hat{\mathbf{e}}_x$. This is why the oscillating dipole moment, having symmetrical scattering in the forward- and back-scattered directions in a Cartesian system has opposite sign in a spherical system. Conversely the direction of the electric field of a radiating quadrupole source is antisymmetric in a Cartesian system with respect to the forward and backward directions, but in the spherical system discussed here, the electric fields have the same sign in the forward and backward directions at a fixed radius. The conclusion we can draw from analysing the complex Mie coefficients is that at the quadrupole frequency, the dipole scattering has a phase difference of π between the field in the forward and backward directions (in spherical coordinates), and the quadrupole has no phase difference, and the phase difference between the two separate modes is approximately 0 for the forward direction and π for the backward direction. This explains why, at the frequency of the quadrupolar mode, the light is scattered almost entirely in the forward direction.

Appendix 2

Finite-element modelling was carried out using HFSS™ (Ansoft). The infinite array was simulated with a unit cell of glass (n=1.5) containing a silver sphere (100 nm diameter) in the

#120946 - $15.00 USD Received 4 Dec 2009; revised 12 Jan 2010; accepted 12 Jan 2010; published 29 Jan 2010

centre. For the angle-dependent simulation, PDMS (n=1.41) filled the lower half-space, just covering the entire sphere. The upper half-space was set as vacuum. The permittivity values for silver were taken from Palik [15] and interpolated using a cubic spline. The height of the unit cell was 1μm and the other two dimensions were varied in order to accommodate changes in the lattice spacing. The top and bottom faces of the unit cell were defined as perfectly matched layers and the global medium was set to be glass for the pitch study, and vacuum for the angle study. For each lattice spacing/incident angle, an initial mesh of tetrahedral cells was created automatically within the modelling package. The mesh was then refined over a number of adaptive passes for a fixed wavelength (400 nm) until the model converged. Typically convergence was obtained for between 30,000 and 50,000 tetrahedra, the exact number depending on the lattice spacing and incident angle. For each lattice spacing and incident angle the mesh from the converged solution at the wavelength of 400 nm was used to calculate the fields for all other wavelengths. When the model had solved, the incident Poynting vector was integrated over the top face of the unit cell and the total Poynting vector (incident + scattered) was integrated over the bottom face. The transmitted intensity was then divided by the incident intensity in order to calculate the transmittance, *T*. For the angle-dependent study the transmittance was evaluated via the appropriate S-parameter (S_{21}) [26]. The optical density is then simply $OD = -\log_{10}(T)$.

The solutions to Mie theory shown in this study were calculated using computer codes based on those provided in the literature [12].

Acknowledgements

This work was supported through funding from QinetiQ in association with Great Western Research (GWR). WLB is funded by a Royal Society Wolfson Research Merit Award.

#120946 - $15.00 USD Received 4 Dec 2009; revised 12 Jan 2010; accepted 12 Jan 2010; published 29 Jan 2010